

Coexistence of local structural heterogeneities and long-range ferroelectricity in Pb-free $(1-x)\text{Ba}(\text{Ti}_{0.8}\text{Zr}_{0.2})\text{O}_3-x(\text{Ba}_{0.7}\text{Ca}_{0.3})\text{TiO}_3$ ceramics

K. Dey,¹ A. Ahad,² K. Gautam,¹ A. Tripathy,¹ S. S. Majid,² S. Francoual,³ C. Richter,⁴ M. N. Singh,⁵ A. Sagdeo,^{5,6} E. Welter,³ N. Vittayakorn,⁷ V. G. Sathe,¹ R. Rawat,¹ and D. K. Shukla^{1,*}

¹UGC DAE Consortium for Scientific Research, University Campus, Khandwa Road, Indore 452001, India.

²Department of Physics, Aligarh Muslim University, Aligarh 202002, India.

³Deutsches Elektronen-Synchrotron (DESY), Notkestrasse 85, D-22607 Hamburg, Germany.

⁴The European Synchrotron Radiation Facility, 71 Avenue des Martyrs, 38000 Grenoble, France.[†]

⁵Synchrotrons Utilization Section, Raja Ramana Centre for Advance Technology, Indore 452013, India.

⁶Homi Bhabha National Institute, Training School Complex, Anushakti Nagar, Mumbai, 400094, India.

⁷Advanced Materials Research Unit, Faculty of Science,

King Mongkut's Institute of Technology Ladkrabang, Bangkok, Thailand 10520.

Environmentally benign $(1-x)\text{Ba}(\text{Ti}_{0.8}\text{Zr}_{0.2})\text{O}_3-x(\text{Ba}_{0.7}\text{Ca}_{0.3})\text{TiO}_3$ (BZT-BCT) ceramics are promising materials due to their remarkable high piezoresponse [Liu and Ren, Phys. Rev. Lett. **103**, 257602 (2009)]. In this Letter, by focusing on local and average structure in combination with macroscopic electromechanical and dielectric measurements we demonstrate the structure property relationship in the tetragonal BZT-BCT ceramic. During high-temperature cubic to tetragonal phase transformation, polar nanoregions are manifested through the spontaneous volume ferroelectricity at temperatures below ~ 477 K. Temperature-dependent local structural investigations across the Zr K edge extended x-ray absorption fine structure spectroscopy reveal an anomalous collaboration between the ZrO_6 and TiO_6 octahedra. These octahedra compromise their individuality during polarization development. The presence of domains of submicron size embedded inside the macroscopic ferroelectric regions below T_m , as well as their hierarchical arrangement, is observed by piezo-response force microscopy. Effects of the existence of the structural/polar heterogeneities below T_m are observed also when polarizabilities of the poled and the unpoled samples are compared; the poled sample is found to be more susceptible to the electric field. In addition, by using electric field dependent x-ray diffraction studies we also show that this ceramic under field exhibits reduction of tetragonal distortion, which is consistent with earlier reports.

I. INTRODUCTION

Investigations on lead-free piezoelectric materials in the last two decades have largely intensified due to environmental concerns. Liu & Ren [1] demonstrated PZT ($\text{PbZr}_x\text{Ti}_{1-x}\text{O}_3$) like ‘morphotropic phase boundary’ (MPB) starting from a triple point in BZT-BCT $(1-x)\text{Ba}(\text{Ti}_{0.8}\text{Zr}_{0.2})\text{O}_3-x(\text{Ba}_{0.7}\text{Ca}_{0.3})\text{TiO}_3$ which possesses ultrahigh piezoresponse (d_{33}) values as high as up to 560-620 pC/N among all lead free compositions. From Liu & Ren [1] and Nahas [2] *et al.*, high piezoresponse has been attributed to isotropic energy flattening along with miniaturization of domains towards the triple point [3]. In addition, domain wall motion was reported to be the dominant extrinsic contribution to high piezoresponse [4]. Electric field dependent x-ray diffraction (XRD) measurements [5] revealed that spontaneous lattice strain reduction enhances domain wall motion in BZT-BCT ceramics. In morphotropic composition (BZT-50BCT) Brajesh *et al.*, [6, 7] showed phase coexistence at room temperature (Tetragonal + Rhombohedral + Orthorhombic) and concluded that electric field induced metastable phases contribute significantly

in high piezoresponse. They also showed relaxor ferroelectric behavior and an ergodic relaxor to normal ferroelectric transformation at $\sim T_m$. Relaxor ferroelectricity i.e., the existence of polar nanoregions (PNRs), a nanoscale inhomogeneity, has been prototypical of highest piezoresponse in Pb-based materials [8–10]. However, in BZT-BCT ceramics, among all possibilities of high piezoresponse, discussed so far, thorough validation of PNRs is yet missing.

In Pb-based perovskite relaxor ferroelectrics, the quenched compositional disorder induced by heterovalent substitution at the B site (e.g. $\text{Pb}(\text{Mg}_{1/3}\text{Nb}_{2/3})\text{O}_3$ - PbTiO_3 , $\text{Pb}(\text{Zn}_{1/3}\text{Nb}_{2/3})\text{O}_3$ - PbTiO_3) generates random fields which break long range ferroelectricity and frustrated interactions among dipoles start to form nanoscale correlations (PNRs) at a higher temperature which is known as the characteristic Burns temperature, T_B [11, 12]. Furthermore, the effect of the Pb positional disorder and its coupling with different BO_6 octahedra also plays a critical role [13, 14]. The PNRs exhibit a large distribution of relaxation times. Divergence of the longest relaxation time takes place at a characteristic temperature, T_f , the freezing temperature [15]. In the ergodic relaxor phase, between two characteristic temperatures (T_B & T_f) PNRs have intrinsic dynamic character and after some percolation limit they transfer into ferroelectric domains just below T_f where macroscopic symmetry changes. However, in the case of canonical relaxors (for

* Corresponding Author: dkshukla@csr.res.in

[†] Now at The Leibniz-Institut für Kristallzüchtung, Max-Born-Straße 2, 12489 Berlin, Germany.

e.g. PMN), the macroscopic symmetry remains the same during ergodic to nonergodic transition, and PNRs show glassy interactions among dipoles in the non-ergodic relaxor phase which transform into ferroelectric domains upon the application of sufficiently large electric field [16].

BaTiO₃-based compositions (e.g. BaZr_xTi_{1-x}O₃, BaSn_xTi_{1-x}O₃, BaHf_xTi_{1-x}O₃) exhibit broad dielectric permittivity maxima with frequency dispersion and characteristic temperatures (T_B & T_f) similar to those Pb-based relaxors [17, 18], and in compositions also the possible existence of PNRs have been reported [19, 20]. However, the origin of PNRs in homovalent substituted BaTiO₃-based compositions is different than in Pb-based (as explained above) and challenging to unravel. A pair distribution function study [21] of BZT (BaZr_xTi_{1-x}O₃) revealed dynamic insights and highlighted the role of Zr in slowing down the B site (Ti) dynamics (responsible for PNRs formation). Therefore, in order to have deeper insights into PNRs in BZT-BCT ceramics it is pivotal to have local structural information about the Zr/Ti ions.

We have chosen a tetragonal composition [(Ba_{0.82}Ca_{0.18})(Ti_{0.92}Zr_{0.08})O₃ (BZT-60BCT)] among the BZT-BCT systems mainly because it is far from the triple point & morphotropic composition. In compositions near triple point and MPB structural instabilities due to the presence of metastable orthorhombic phases [7, 22] and nearly vanishing anisotropy induced domain wall motion [5] may inhibit the study of intrinsic features of PNRs, which are hiding in these ceramics.

In this letter, we demonstrate that, in BZT-60BCT below T_m , local structural heterogeneities coexist with long range ferroelectricity and this coexistence leads to hierarchical arrangements of micro and nano domains inside large ferroelectric domains. We also show direct evidences of PNRs above T_m . Our detail local structural studies of TiO₆ and ZrO₆ reveal a peculiar behavior of these two octahedra during polarization development and static disorder in Zr-O bonds below T_m .

II. EXPERIMENTS

The ceramic BZT-60BCT has been synthesized by conventional solid state reaction using high-purity chemicals; BaCO₃ (99.9%), CaCO₃ (99.9%), TiO₂ (99.9%), and ZrO₂ (99.7%). Stoichiometrically mixed powders were thoroughly ball milled and calcined at 1300°C for 4 h. Sintering was performed at ~1540°C for 2 h in air. XRD measurement was done using Bruker D2 Phaser X-ray diffractometer utilizing Cu K_α radiation. Dielectric measurements were performed utilizing HIOKI LCR meter (IM 3536) and a CRYOCON temperature controller. Polarization-electric field (P-E) hysteresis loops were measured by Radiant precision premier II loop tracer. Temperature dependent XRD measurements were carried out at BL12 beamline at Indus II, RRCAT, India, by utilizing photons of ~ 14.87 keV (0.834 Å) in θ - 2θ geometry during the heating cycle from room tem-

perature up to 575 K. The Raman measurements were carried out using a Horiba JY model HR-800 single spectrometer with high resolution grating and a CCD detector by using a 473 nm laser beam in backscattering geometry. Electric field dependent x-ray diffraction was performed using high-energy photons (~37 keV) in transmission geometry at beamline P09 at PETRA III at DESY (Hamburg, Germany). A PerkinElmer two-dimensional detector was used at a fixed distance of ~ 650 mm. For poled measurements the sample was poled at ~40°C for 30 min at 1 kV/mm and then field cooled down to room temperature. After ~ 24 hours of aging of the poled samples, piezoelectric charge coefficient d_{33} was monitored by a commercial d_{33} meter from APC. A similar poling strategy was adopted for all other poled measurements. EXAFS (extended X-ray absorption fine structure) measurements at the Zr K edge in transmission and Ti K edge XANES (X-ray absorption near edge structure) in fluorescence were collected at P65 beamline of PETRA-III synchrotron. Piezo-response force microscopy (PRFM) measurements were carried out on mirror finished polished surfaces. The sample was annealed at 350°C for 2 hrs to remove stresses induced by polishing. PRFM measurements were carried out using a fiber interferometry based low temperature scanning probe microscope system from AttocubeTM, Germany. A PtSi-FMTM conducting cantilever from NanosensorsTM was used for scanning sample surface. Topography was measured in contact mode along with simultaneous measurement of piezo-response at an applied ac voltage of 10 V (peak to peak) at 41.33 kHz.

III. RESULTS

The room temperature tetragonal structure of BZT-60BCT has been confirmed using XRD (see Fig. S1 in the supplemental material [23]). The real and imaginary parts of the dielectric permittivity show diffused dielectric maxima at ~ 380 K (see Fig. 1 (a) & (b)), signatures of relaxor ferroelectricity. Inset (ii) in Fig. 1(b) shows that the inverse permittivity deviates from the Curie-Weiss law at ~ 477 K, which indicates a characteristic Burn's temperature, T_B [24]. The diffusion exponent (γ) and diffuseness (δ) of permittivity peak are calculated from the fit (see inset (i) in 1 (b)) using an empirical formula from reference [25], $\frac{\epsilon_m}{\epsilon} = 1 + \frac{(T-T_m)^\gamma}{2\delta^2}$, where T_m is the peaking temperature at selected frequency. Obtained fitting parameters are $\gamma = 1.52$ & $\delta = 8.7$ K. The polarization-electric field (P-E) hysteresis loop in Fig. 1(c) exhibits coercive field (E_C) ~ 4 kV/cm and remanence ~ 10 μ C/cm². The temperature dependent remanence (see inset in Fig. 1(c)) is plotted from P-E loop measurements done at various temperatures [23] and shows a non zero value of polarization even above T_m ~ 380 K. The observations of Burn's temperature and non-zero value of polarization above T_m indicate the existence of PNRs at temperatures above T_m . A longi-

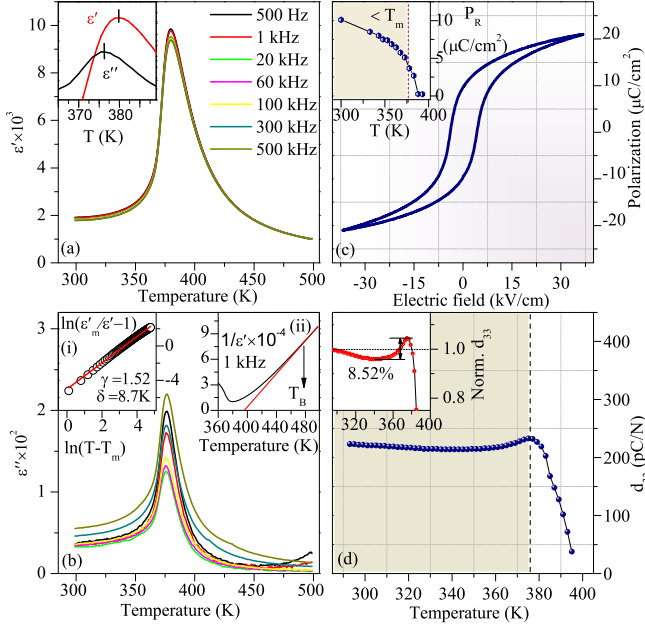


FIG. 1. Temperature dependence of (a) the real & (b) imaginary parts of relative permittivity at different frequencies. The inset in (a) shows the zoomed portion of real and imaginary permittivities near the peak at 1 kHz. The bars indicate that T_m for the imaginary part is at a lower temperature than that of the real part. Inset (ii) in (b) shows the Curie-Weiss fit of the real permittivity indicates a deviation from the temperature marked T_B (~ 477 K), and the inset (i) in (b) shows the linear fitting by using the empirical formula (see text). (c) Polarization- electric field hysteresis loop at room temperature; and inset shows the temperature dependence of the remnant polarization. (d) Temperature-dependent d_{33} ; the inset shows normalized d_{33} with temperature and arrow indicates the maximum percentage change in d_{33} .

tudinal piezoelectric coefficient (d_{33}) of ~ 223 pC/N and its temperature insensitivity up to ~ 375 K can be radially seen in Fig. 1(d); the inset shows normalized d_{33} with temperature and its maximum variation is found to be only $\sim 8.52\%$, which is better than requirement ($\sim 10\%$) for applications.

To further substantiate the presence of PNRs and to have insights of these characteristic temperatures (T_B & T_m) observed in macroscopic electrical measurements we now focus on structural studies results obtained using synchrotron XRD measurements as a function of temperature (300 K to 575 K). Fig. 2 (a) shows that high temperature pseudocubic (PC) reflections $(200)_{PC}$ & $(220)_{PC}$ split with decreasing temperature in $(200)_T/(002)_T$ and $(220)_T/(202)_T$, respectively, signifying a structural phase transition from cubic to tetragonal.

Rietveld refinement is done by using the Fullprof program [26] with space group P4mm from RT to 375 K and with the space group Pm-3m from 400 K up to 575 K (see Fig. S1 in supplemental material [23]). Fig. 2

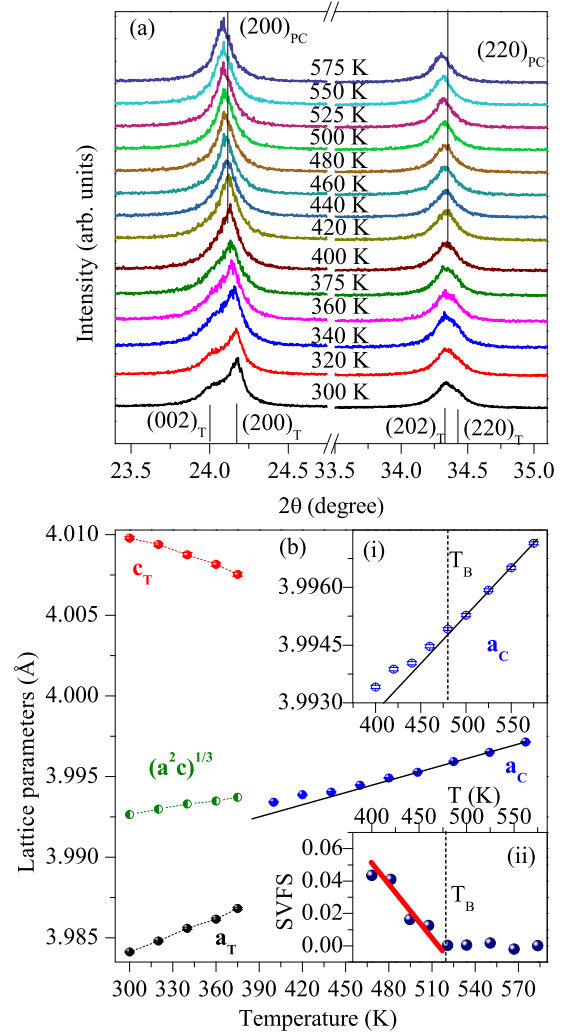


FIG. 2. (a) Temperature dependence of reflections $(200)_{PC}$ & $(220)_{PC}$. (b) Temperature variation of lattice parameters in tetragonal and cubic structures. Inset (i) in (b) shows the zoomed portion of the cubic lattice parameters' temperature dependence. Inset (ii) in (b) shows the calculated spontaneous volume ferroelectrostriction (SVFS) with temperature.

(b) shows the temperature dependence of the refined lattice parameters. Transitions in lattice parameter trend clearly matches with the dielectric maxima temperature (T_m) (see Fig. 1 (a)). Interestingly, the inset (i) in Fig. 2(b) shows deviation of the cubic lattice parameters at ~ 477 K temperature (identified also as Burn's temperature T_B , see inset (ii) in Fig. 1 (b)). These observed anomalies in structural parameters can be understood as follows. Ferroelectric order overcomes the decrease of anharmonic lattice phonon vibration and results into dilatation of cubic lattice parameter and this effect is termed as spontaneous volume ferroelectrostriction (SVFS) [27]. Here, in the cubic phase temperature behavior of the observed volume V_{exp} is found to deviate at ~ 477 K from its usual behavior V_{nm} . The SVFS is calculated by using

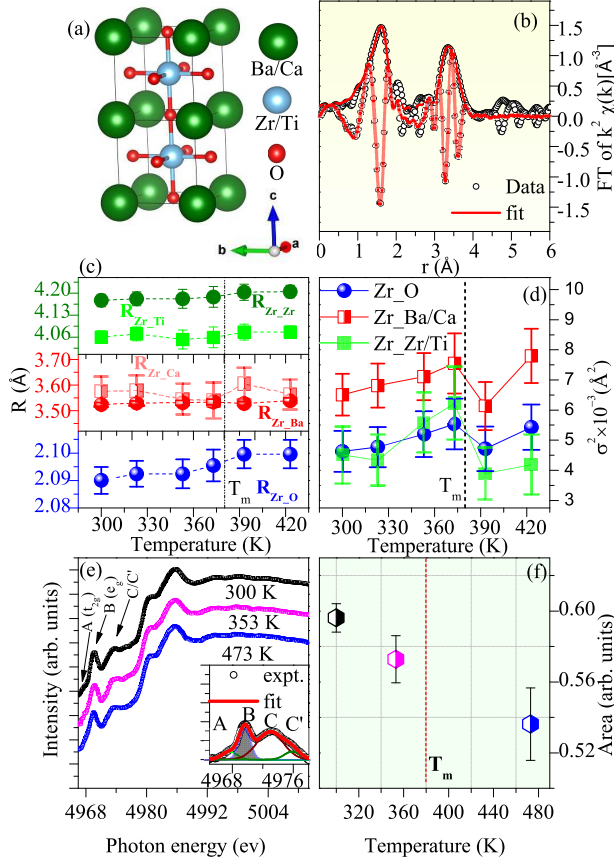


FIG. 3. (a) Standard perovskite model, which is used in the EXAFS fit. (b) Data and fit of the modulus and imaginary part of the Fourier transform in r space at room temperature. (c) Temperature dependent coordination distances and (d) mean-square relative displacement (msrd) parameters involved in the fitting of the Zr K-edge EXAFS. (e) The Ti K-edge XANES spectra at different temperatures; the inset shows fitting of the preedge peak at room temperature. (f) Temperature dependence of the integrated intensity of feature B (e_g) in (e).

the equation $\omega_s = (V_{exp} - V_{nm}) / V_{nm} \times 100\%$, from references [27, 28] shown in the inset (ii) of Fig. 2 (b). Evolution of SVFS just below T_B (~ 477 K) (inset (ii) in Fig. 2 (b)) signifies the onset of polarization as well as clearly indicates the existence of PNRs [8, 27, 28]. Motivated by the above discussed results about evidences of PNRs, now we try to figure out the interplay between the Zr local structure and the PNRs. The Zr local structure are investigated by performing the Zr K-edge EXAFS measurements at selected temperatures across T_m and the results are shown in the Fig. 3. We have used standard perovskite model (see Fig. 3(a)) with linear Zr-O-Zr, Zr-O-Ti links during fitting as has been used earlier in BZT compositions [29]. During temperature dependent EXAFS analysis we have utilized the stoichiometric ratio of Ba/Ca and Ti/Zr obtained from fit at 300 K, which are found nearby nominal composition values (see details

of the EXAFS analysis in [23]). The fitted Zr K-edge EXAFS spectra at room temperature is shown in Fig. 3(b). From the results of first coordination shell we have found that Zr-O bond distance increases significantly with temperature (see Fig. 3(c)). The Zr-Ba & Zr-Ca interatomic distances are not same at room temperature. As temperature increases both the parameters (R_{Zr-Ba} , R_{Zr-Ca}) come closer, while approaching T_m . The Zr-Ba interatomic distance (~ 3.54 Å) is found significantly lesser than one in $BaZrO_3$ (~ 3.64 Å) [30] i.e., the ZrO_6 octahedra are not in an ideal cubic environment. Additionally, the Ti-O bond distance (~ 1.97 Å) is found to be shorter compared to the Zr-O bond distance (~ 2.09 Å). In order to better understand the local picture, we are turning our attentions to the mean square relative displacement (msrd) parameters as it contains information about thermal disorder as well as static disorder of all scattering paths involved. Fig. 3 (d) shows evolution of msrd (σ_{Zr-O}^2) with temperature. The σ_{Zr-O}^2 at room temperature is higher in this system as compare to that of $BaZrO_3$ [30]. So, here, the Zr-O bonds contain an additional disorder other than thermal disorder (Einstein's model) [31, 32]. Earlier [30], in case of $BaZr_xTi_{1-x}O_3$, presence of a temperature independent static disorder together with thermal disorder was attributed to the distortion of ZrO_6 octahedra or tiny displacement of the Zr atoms. Additionally, at $\sim T_m$, σ_{Zr-O}^2 shows anomaly which is not seen earlier in case of BZT. Again, below T_C behavior of the $\sigma_{Zr-Ti/Zr}^2$ with temperature is more steeper compared to the σ_{Zr-O}^2 & $\sigma_{Zr-Ba/Ca}^2$. This indicates modifications in linkage between the Zr-O and the O-Ti bonds due to decreasing covalent character of the Ti-O bonds. This is supported by a direct evidence of decreasing hybridization between the Ti and the O with temperature seen in the Ti K-edge X-ray absorption near edge structure (XANES) spectra (see Fig. 3 (e,f)). The features A and B, in Fig. 3 (e), are ascribed to t_{2g} and e_g , respectively and C/C' correspond to local Zr/Ti ratio surrounding absorber atom. The intensity of feature B (e_g), which is related to Ti-O hybridization, decreases with temperature (Fig. 3(f)), and confirms that with increasing temperature in this range strength of the Ti-O hybridization is weakening. Above T_m , $\sigma_{Zr-Ti/Zr}^2$ is more stable compared to other msrd parameters. Such temperature evolution of $\sigma_{Zr-Ti/Zr}^2$ suggests disorder along the Zr-O-Ti links which detains phonon activation. At around T_m , σ_{Zr-O}^2 also shows anomaly, indicating direct involvement of the Zr local structure on polarization. Based on our results from local structural analysis and the NPDF results by Pramanick *et al.*, [21] we can say that presence of the Zr affects surrounding Ti ions with the tensile stress on it and can change the polarization (by slowing down dynamics of Ti^{4+} ions). In order to understand the effect of these local structural heterogeneities on long range polar order below T_m we have also performed the dielectric measurements on poled sample and compared the results with

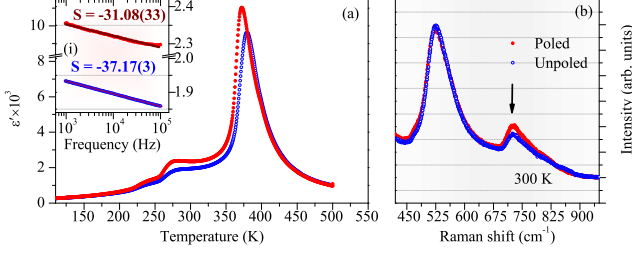


FIG. 4. (a) Temperature-dependent dielectric permittivity of poled and unpoled samples (at 1 kHz) taken during heating cycles. The inset shows the linearly fitted dielectric dispersion of poled and unpoled samples at room temperature. (b) Raman spectra (vertically translated for overlapping) of poled and unpoled samples at room temperature.

that of unpoled sample. The dielectric dispersion or difference in permittivity at two frequencies is a measure of the degree of polar heterogeneity in a system [33, 34]. In general, the dielectric dispersion is less for long range ferroelectric materials and it increases for material that shows relaxor ferroelectric behavior which are complex perovskite (ABO_3) system with different cations present in the same site (A or B site). Relaxor ferroelectrics (i.e. BNT, BNT-BKT etc.) or canonical relaxors (i.e. PMN, PZN) can be transformed into long range polar order by the application of sufficiently high electric field, therefore dielectric dispersion as well as polar heterogeneity get decreased. As we see from EXAFS results that the studied composition exhibits significant disorder due to different sizes' cations are present at both the A and the B sites, so a comparison of dielectric dispersion in poled and unpoled sample can directly tell about the degrees of polar heterogeneities. The inset of Fig. 4(a) shows that the dielectric dispersion decreases significantly for poled sample therefore it is inferred that the degree of polar heterogeneity is reduced after poling. These observation of presence of polar heterogeneities in the unpoled sample can be correlated to structural heterogeneities observed in the EXAFS experiment.

Surprisingly, dielectric permittivity enhances in case of poled sample which can be visibly seen from Fig. 4(a). Generally, by applying electric field on ferroelectric domains, polarization coherence increases along field direction and the sample becomes less susceptible to smaller ac field and thereby dielectric permittivity reduces [35, 36]. Similar is true in case of canonical relaxors (PMN, PZN) [37] or in the nonergodic phase of relaxor ferroelectrics (e.g. BNT based systems) below T_m [34, 38]. However, field induced real permittivity enhancement is reported to exist below T_m in case of PMN-PT, and that has been attributed to synergistic interaction among ferroelectric domains and PNRs [39], as may be the case here too. We also performed Raman measurements on the poled and the unpoled samples (see Fig. 4(b)). The Raman spectra of these samples match well with the previous

reports [40–42]. The Raman spectra of this sample as well as other samples of BZT-xBCT series ($x = 0.3, 0.5, 0.6, 0.7$) are compared and presented in supplementary [23]. The Raman mode at $\sim 522 \text{ cm}^{-1}$ (see Fig. 4(b) and Fig. S4 in [23]) have dominant $A_1(\text{TO})$ behavior and is related to BO_6 octahedra [43]. The Raman mode $A_1(\text{LO})/\text{E}(\text{LO})$ at $\sim 720 \text{ cm}^{-1}$ is key signature related to the long range ferroelectricity [44, 45]. Both of these modes are present in all BaTiO_3 -based systems. The intensity of the Raman mode (at $\sim 720 \text{ cm}^{-1}$) enhances after poling and suggests that long range ferroelectricity has indeed enhanced after poling [43, 44]. Therefore, both these measurements (dielectric and Raman) clearly suggest that there exist nanoscale polar inhomogeneities along with long range ferroelectricity below T_m and reduces marginally in poled sample.

In order to visualize these local structural heterogeneities we have also performed the domain imaging by PRFM. The PRFM is a technique based on the detection of local converse piezoelectric effect and this is promising for imaging fine scale domains [46–48]. Fig. 5 (a) shows the surface morphology of the polished sample by scanning a $2 \times 2 \mu\text{m}^2$ region. Fig. 5 (b) & (c) show the piezoelectric amplitude and PRFM phase of the same scanned region. Ferroelectric domains of different orientations with different contrast can be clearly seen in Fig. 5 (b) & (c). Nanoscale domain configurations (marked by dot circles) are observed for this composition within the large ferroelectric domain (see Fig. 5 (b)). Fig. 5 (d) shows the hierarchical domain configuration and is similar to the earlier reports resulting due to the interplay of stress accommodation and polarization compensation [49–52]. Fig. 5 (e) shows the piezoelectric amplitude hysteresis loop which was obtained by applying electric field along the tip axis on selected region. The butterfly like piezoelectric amplitude hysteresis loop confirms the existence of well defined polarization along field direction. Historically, high piezoresponse is always associated with hierarchical domain structure or complex microstructure with a combination of microdomains and nanodomains as these domains can easily respond to the external stimulus [50, 53, 54]. The complex domain configuration of this sample is compatible with its high piezoresponse ($\sim 223 \text{ pC/N}$) [53, 54].

Finally, for the sake of completeness we carried out X-ray diffraction (at $\sim 300 \text{ K}$, below T_m) in presence of field up to $\pm 6.7 \text{ kV/cm}$ ($\sim 1.67E_c$) and quantified the structural changes under electric field. Electric field was applied on sample at an angle of 45° with respect to the incident X-ray beam. This filters out effects of ferroelastic domain induced texturing and also assures reliability of the structural information through the Rietveld refinement [55]. Fig. 6(a) shows the fitted XRD pattern, which is in good agreement with the experimental data. Fig. 6(b) shows tetragonal distortion with electric field, though small. The observed tetragonal distortion reduction clearly indicates the electric field induced 90° domain wall motion by reduction of anisotropy. In the

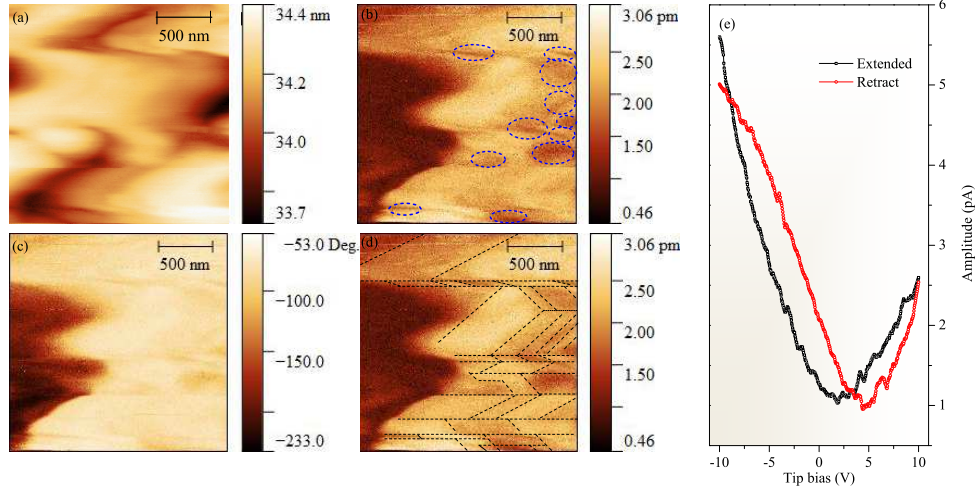


FIG. 5. (a) Topography, (b) piezoelectric amplitude, and (c) PRFM phase images of the same $2 \times 2 \mu\text{m}^2$ scan area, at room temperature. The circles in (b) indicate different nanoscale domains. (d) Hierarchy of domains and subdomains marked by dashed lines and (e) local PRFM amplitude hysteresis loop with electric field.

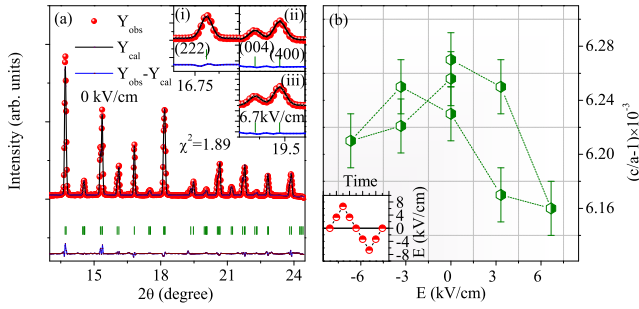


FIG. 6. (a) Rietveld refined X-ray diffraction pattern at zero electric field at room temperature. Insets (i) and (ii) in (a) show zoomed singlet $(222)_{pc}$ and doublet $(400)_{pc}$ peaks at zero field, and inset (iii) shows doublet $(400)_{pc}$ peak at 6.67 kV/cm. (b) Tetragonal distortion vs. electric field shows an inverted butterfly like feature. A bipolar electric field was applied as shown in the inset of (b).

Pb-based compositions, tetragonal distortion reduces by enhancing the monoclinic phase fraction [55–57]. However, in the present case no traces of monoclinicity is observed. Zoomed portions around (004) and (400) under highest electric field is depicted in inset (iii) of Fig. 4(a) and no extra features are observed, as is the case in Pb-based compounds. Our electric field dependent XRD results and conclusions are well in agreement with those already reported on the same composition [5, 58]

IV. DISCUSSION

BZT-60BCT is found to exhibit a weaker dielectric dispersion at around T_m compare to the canonical re-

laxors PMN and PZN; however, other characteristics of relaxor type exist, e.g., a temperature of the real permittivity maxima (~ 380 K) significantly higher than that of the imaginary permittivity maxima (~ 375 K), deviation from the C-W law at a temperature (at ~ 477 K) much higher than T_m , and the presence of a slim hysteresis loop above T_m . The diffusion exponent of this system ($\gamma=1.52$) suggests that this system exhibits diffused ferroelectric phase transition, an intermediate between classical ferroelectric ($\gamma=1$) and canonical relaxor ($\gamma=2$) [59]. Therefore, this system is analogically similar to PMN-PT and PZN-PT compositions near the MPB [39, 60]. The dielectric anomalies (deviation from C-W law and structural phase transition around T_m) are successfully justified by temperature dependent XRD. The appearance of SVFS at ~ 477 K which is associated with the onset of the PNRs is in accordance with other perovskite (ABO_3) ferroelectrics [27] in which polarization developments also take place due to the relative displacements of the cations and anions.

The origin of nanodomains here may relate due to the inhomogeneities in the local structure and in strain (cations with different sizes) which break the long-range polar order. The compositions studied here are perfect candidate for such a scenario because these are highly disordered compound as it involves Zr^{4+} (ionic radii $r \sim 0.72\text{\AA}$) substitution in place of Ti^{4+} ($r \sim 0.61\text{\AA}$) and Ca^{2+} ($r \sim 1.34\text{\AA}$) in place of Ba^{2+} ($r \sim 1.61\text{\AA}$) and thus large ionic radii [61] differences at both sites. Weakening of long range polar-order as a function of the Zr and Ca content in these compositions is experimentally evidenced by our Raman measurements, for which we have compared the four different compositions of BZT-xBCT ($x = 0.3, 0.5, 0.6, 0.7$) [23]. The $A_1(\text{TO})$ phonon mode [43, 44], related to polar Ti-O vibrations (at $\sim 270 \text{ cm}^{-1}$), clearly becomes weaker and broader for Ca^{2+} rich BZT-

BCT systems.

Unlike Pb-based relaxors in which Pb positional disorder plays an important role, in BZT-BCT it has been reported [42] that at the A site (Ba/Ca) there is no significant disorder. However, from our Zr local structural studies we have found a significant difference between R_{Zr-Ba} and R_{Zr-Ca} which together with our Raman results highlights that the A site (Ba/Ca) also contributes to local structural heterogeneities. Recent first-principle studies [62, 63] also highlighted the steric effect induced B-site to A-site ferroelectricity transformation by incorporating lower ionic radii Ca in Ba sites. However, to shed light on the peculiar role of Ca more experimental investigations are necessary.

In PZT ceramics relaxor behavior is absent, although the same Ti and Zr cations are present in the B sites as in BZT. This is mainly because, the A site cations possess a contrasting character. The stereochemically active lone pairs of Pb in covalently bonded Pb-O result in large off centering in their respective oxygen dodecahedra, whereas ionic-type bonding between the Ba-O results in almost no shifting of Ba. In Pb-based system, Pb positional disorder couples differently with different BO_6 octahedra; strong correlations between the cations make $PbTiO_3$ ferroelectric and $PbZrO_3$ antiferroelectric [64–66]. In BZT-BCT substitution of Ca at the Ba sites, however, increases the A site bond strain due to a large ionic radii mismatch between Ba and Ca; however, the effect of the Ca on the BO_6 octahedra is not as prominent as that of Pb. In $BaTiO_3$ -based systems (BT, BZT, BST) polarization appears mainly due to the Ti^{4+} and the effect of dopant ions in $BaTiO_3$ system exhibits diffuse scattering by setting up random strain fields generating frustrated PNRs [19], whereas PZT does not show diffuse scattering [67]. Moreover, in $BaTiO_3$ -based relaxors B site substitution has a more important role in setting up local strains by decreasing transverse correlations and creating frustration during long-range polar order [19]. Fanoresonance and the thermally activated THz relaxation mode [68] due to the difference in off-centering of Zr^{4+} and Ti^{4+} is attributed as the cause of PNRs or relaxor behavior in BZT [69]. The Ti^{4+} dynamics are reported to exist even in the non-ergodic relaxor phase of BZT [70, 71].

Generally for non-ergodic relaxors (below T_m) dielectric dispersion is larger (compare to long range ferroelectrics), and application of a sufficiently high electric field results in a reduction of dielectric dispersion. Dispersion in the permittivity data signifies the degree of polar inhomogeneity [33, 34]. Here, in this system, dispersion in the real permittivity is also present well below T_m . The slopes calculated from dielectric permittivity variation with frequency (inset in Fig. 4(a)) suggest that significant polar inhomogeneity is present in case of the unpoled specimen and it decreases only marginally after electric poling [23]. Normally, the presence of PNRs below T_m is expected to show nonergodicity [16] and application of electric field results in the reduction of real

permittivity, which here is counter-intuitive[34]. Further, both, PNRs and ferroelectric domains individually are reported to show enhancement of polarization coherence after poling thereby a reduction in the dielectric constant [36, 72, 73]. In contrary, Li *et al.*, [39] highlighted dielectric constant enhancement after poling as the cornerstone of ultrahigh piezoelectricity. The temperature evolution of structural transformations of PNRs at lower temperature, and colinear arrangement of PNRs at higher temperature were attributed to dielectric as well as piezo amplification in PNR-ferroelectric composites [39]. In our case also, in the poled sample real permittivity increases significantly ($\sim 23\%$). We speculate that similar kinds of interactions are involved in this system, as explained by Li *et al* [39]. Our PRFM measurements show the presence of polar nanodomains at room temperature and support our conjecture.

V. CONCLUSIONS

In summary, by combining a set of local and average structural studies on a tetragonal BZT-BCT ceramic we have presented the relationship between local structural heterogeneities in it and its macroscopic dielectric, ferroelectric and piezoelectric properties. Temperature dependent XRD confirms tetragonal to cubic phase transition at $\sim T_m$ (380 K). Furthermore, the onset of spontaneous volume ferroelectrostriction and deviation from the C-W law (at $T_B \sim 477$ K), slim hysteresis and dielectric dispersion confirm the presence of PNRs from 477 K in this composition. The Zr local structural investigations confirm that the ZrO_6 & TiO_6 octahedra retain the individuality of their respective parent compounds (i.e, $BaZrO_3$ and $BaTiO_3$) and ZrO_6 octahedra are found to have direct involvement during polarization development. The larger ZrO_6 octahedra create tensile stress on surrounded TiO_6 octahedra and the presence of static disorder in Zr-O bonds produces local structural heterogeneities; during polarization development the ZrO_6 octahedra distort. Local structural heterogeneities try to break the long-range polar order by forming nanoscale hierarchical domains. These domains are evidenced by PRFM and are supposed to be responsible for the enhancement of real permittivity ($\sim 23\%$) after poling. Additionally, high resolution SXRD confirms also the electric field induced reduction of tetragonal distortion in this ceramic.

ACKNOWLEDGMENTS

K.D., A.A. and D.K.S gratefully acknowledge the financial support from the Department of Science and Technology (DST) in India through the India-DESY collaboration for performing experiments at PETRA-III, DESY. The authors acknowledge S. Yadav for help with P-E loop measurements, and A. Yadav for help with EXAFS data analysis. D. Reuther is acknowledged for set-

ting up the voltage source used in the electric field dependent XRD measurements. C.R. acknowledges the sup-

port from the project CALIPSOplus under Grant Agreement No. 730872 from the EU Framework Programme for Research and Innovation HORIZON 2020.

-
- [1] W. Liu and X. Ren, Large piezoelectric effect in pb-free ceramics, *Physical review letters* **103**, 257602 (2009).
 - [2] Y. Nahas, A. Akbarzadeh, S. Prokhorenko, S. Prosandeev, R. Walter, I. Kornev, J. Íñiguez, and L. Bellaiche, Microscopic origins of the large piezoelectricity of leadfree (ba, ca)(zr, ti) o 3, *Nature communications* **8**, 15944 (2017).
 - [3] J. Gao, Y. Dai, X. Hu, X. Ke, L. Zhong, S. Li, L. Zhang, Y. Wang, D. Wang, Y. Wang, *et al.*, Phase transition behaviours near the triple point for pb-free (1- x) ba (zr0. 2ti0. 8) o3-x (ba0. 7ca0. 3) tio3 piezoceramics, *EPL (Europhysics Letters)* **115**, 37001 (2016).
 - [4] J. Gao, X. Hu, L. Zhang, F. Li, L. Zhang, Y. Wang, Y. Hao, L. Zhong, and X. Ren, Major contributor to the large piezoelectric response in (1- x) ba (zr0. 2ti0. 8) o3- x (ba0. 7ca0. 3) tio3 ceramics: Domain wall motion, *Applied Physics Letters* **104**, 252909 (2014).
 - [5] G. Tutuncu, B. Li, K. Bowman, and J. L. Jones, Domain wall motion and electromechanical strain in lead-free piezoelectrics: Insight from the model system (1-x) ba (zr0. 2ti0. 8) o3-x (ba0. 7ca0. 3) tio3 using in situ high-energy x-ray diffraction during application of electric fields, *Journal of Applied Physics* **115**, 144104 (2014).
 - [6] K. Brajesh, K. Tanwar, M. Abebe, and R. Ranjan, Relaxor ferroelectricity and electric-field-driven structural transformation in the giant lead-free piezoelectric (ba, ca)(ti, zr) o 3, *Physical Review B* **92**, 224112 (2015).
 - [7] K. Brajesh, M. Abebe, and R. Ranjan, Structural transformations in morphotropic-phase-boundary composition of the lead-free piezoelectric system ba (t i 0.8 z r 0.2) o 3-(b a 0.7 c a 0.3) ti o 3, *Physical Review B* **94**, 104108 (2016).
 - [8] L. E. Cross, Relaxor ferroelectrics, *Ferroelectrics* **76**, 241 (1987).
 - [9] M. E. Manley, D. L. Abernathy, R. Sahul, D. E. Parshall, J. W. Lynn, A. D. Christianson, P. J. Stonaha, E. D. Specht, and J. D. Budai, Giant electromechanical coupling of relaxor ferroelectrics controlled by polar nanoregion vibrations, *Science advances* **2**, e1501814 (2016).
 - [10] S.-E. Park and T. R. Shrout, Ultrahigh strain and piezoelectric behavior in relaxor based ferroelectric single crystals, *Journal of Applied Physics* **82**, 1804 (1997).
 - [11] A. Bokov and Z.-G. Ye, Recent progress in relaxor ferroelectrics with perovskite structure, *Journal of materials science* **41**, 31 (2006).
 - [12] G. Burns and F. Dacol, Glassy polarization behavior in ferroelectric compounds pb (mg13nb23) o3 and pb (zn13nb23) o3, *Solid state communications* **48**, 853 (1983).
 - [13] C. Perrin, N. Menguy, E. Suard, C. Muller, C. Caranoni, and A. Stepanov, Neutron diffraction study of the relaxor-ferroelectric phase transition in disordered pb (sc1/2nbl/2) o3, *Journal of Physics: Condensed Matter* **12**, 7523 (2000).
 - [14] P. S. Halasyamani, Asymmetric cation coordination in oxide materials: Influence of lone-pair cations on the intra-octahedral distortion in d0 transition metals, *Chemistry of materials* **16**, 3586 (2004).
 - [15] R. Pirc and R. Blinc, Vogel-fulcher freezing in relaxor ferroelectrics, *Physical review B* **76**, 020101 (2007).
 - [16] A. A. Bokov and Z.-G. Ye, Dielectric relaxation in relaxor ferroelectrics, *Journal of Advanced dielectrics* **2**, 1241010 (2012).
 - [17] A. Simon and J. Ravez, Relations between relaxor behavior and cationic substitutions in lead-free batio3 derived ceramics, *Ferroelectrics* **240**, 1601 (2000).
 - [18] Y. Huang, C. Zhao, B. Wu, and J. Wu, Multifunctional batio3-based relaxor ferroelectrics toward excellent energy storage performance and electrostrictive strain benefiting from crossover region, *ACS Applied Materials & Interfaces* **12**, 23885 (2020).
 - [19] Y. Liu, R. Withers, B. Nguyen, and K. Elliott, Structurally frustrated polar nanoregions in ba ti o 3-based relaxor ferroelectric systems, *Applied physics letters* **91**, 152907 (2007).
 - [20] L. Xie, Y. Li, R. Yu, Z. Cheng, X. Wei, X. Yao, C. Jia, K. Urban, A. Bokov, Z.-G. Ye, *et al.*, Static and dynamic polar nanoregions in relaxor ferroelectric ba (ti 1- x sn x) o 3 system at high temperature, *Physical Review B* **85**, 014118 (2012).
 - [21] A. Pramanick, W. Dmowski, T. Egami, A. S. Budisuharto, F. Weyland, N. Novak, A. D. Christianson, J. Borreguero, D. L. Abernathy, and M. R. V. Jørgensen, Stabilization of polar nanoregions in pb-free ferroelectrics, *Physical review letters* **120**, 207603 (2018).
 - [22] A. Akbarzadeh, K. Brajesh, Y. Nahas, N. Kumar, S. Prokhorenko, D. Swain, S. Prosandeev, R. Walter, I. Kornev, J. Íñiguez, *et al.*, Quantum-fluctuation-stabilized orthorhombic ferroelectric ground state in lead-free piezoelectric (ba, ca)(zr, ti) o 3, *Physical Review B* **98**, 104101 (2018).
 - [23] See Supplemental Material at for details about the structural characterization, P-E hysteresis measurements, dielectric and diffusion exponent in the poled sample, Raman spectra and EXAFS analysis.
 - [24] G. Burns and F. Dacol, Crystalline ferroelectrics with glassy polarization behavior, *Physical Review B* **28**, 2527 (1983).
 - [25] A. Bokov, Y.-H. Bing, W. Chen, Z.-G. Ye, S. Bogatina, I. Raevski, S. Raevskaya, and E. Sahkar, Empirical scaling of the dielectric permittivity peak in relaxor ferroelectrics, *Physical Review B* **68**, 052102 (2003).
 - [26] J. Rodríguez-Carvajal, An introduction to the program fullprof, Laboratoire Leon Brillouin (CEA-CNRS) (2001).
 - [27] J. Chen, L. Hu, J. Deng, and X. Xing, Negative thermal expansion in functional materials: controllable thermal expansion by chemical modifications, *Chemical Society Reviews* **44**, 3522 (2015).

- [28] J. Chen, F. Wang, Q. Huang, L. Hu, X. Song, J. Deng, R. Yu, and X. Xing, Effectively control negative thermal expansion of single-phase ferroelectrics of PbTiO_3 -(Bi, La) FeO_3 over a giant range, *Scientific reports* **3**, 2458 (2013).
- [29] I. Levin, E. Cockayne, V. Krayzman, J. C. Woicik, S. Lee, and C. A. Randall, Local structure of $\text{Ba}(\text{Ti}, \text{Zr})\text{O}_3$ perovskite-like solid solutions and its relation to the band-gap behavior, *Physical Review B* **83**, 094122 (2011).
- [30] C. Laulhé, F. Hippert, J. Kreisel, M. Maglione, A. Simon, J. Hazemann, and V. Nassif, Exafs study of lead-free relaxor ferroelectric $\text{Ba}_{1-x}\text{Zr}_x\text{O}_3$ at the Zr K edge, *Physical Review B* **74**, 014106 (2006).
- [31] P. Fornasini and R. Grisenti, On exafs debye-waller factor and recent advances, *Journal of synchrotron radiation* **22**, 1242 (2015).
- [32] G. Beni and P. Platzman, Temperature and polarization dependence of extended x-ray absorption fine-structure spectra, *Physical Review B* **14**, 1514 (1976).
- [33] P. B. Groszewicz, M. Gröting, H. Breitzke, W. Jo, K. Albe, G. Buntkowsky, and J. Rödel, Reconciling local structure disorder and the relaxor state in $(\text{Bi}_{1/2}\text{Na}_{1/2})\text{TiO}_3$ - BaTiO_3 , *Scientific reports* **6**, 31739 (2016).
- [34] G. D. Adhikary, D. K. Khatua, A. Senyshyn, and R. Ranjan, Random lattice strain and its relaxation towards the morphotropic phase boundary of $\text{Na}_{0.5}\text{Bi}_{0.5}\text{TiO}_3$ -based piezoelectrics: Impact on the structural and ferroelectric properties, *Physical Review B* **99**, 174112 (2019).
- [35] P. Yadav, S. Sharma, and N. Lalla, Coexistence of domain relaxation with ferroelectric phase transitions in BaTiO_3 , *Journal of Applied Physics* **121**, 184101 (2017).
- [36] K. C. Koa, Dielectric phenomena in solids with emphasis of physical concepts of electronic processes (2004).
- [37] Y. Zhang, J. Tian, L. Li, and Z. Gui, Influences of dc and ac fields on the dielectric properties of relaxor ferroelectric ceramics, *Journal of Materials Science: Materials in Electronics* **11**, 347 (2000).
- [38] B. N. Rao, R. Datta, S. S. Chandrashekar, D. K. Mishra, V. Sathe, A. Senyshyn, and R. Ranjan, Local structural disorder and its influence on the average global structure and polar properties in $\text{Na}_{0.5}\text{Bi}_{0.5}\text{TiO}_3$, *Physical Review B* **88**, 224103 (2013).
- [39] F. Li, S. Zhang, T. Yang, Z. Xu, N. Zhang, G. Liu, J. Wang, J. Wang, Z. Cheng, Z.-G. Ye, *et al.*, The origin of ultrahigh piezoelectricity in relaxor-ferroelectric solid solution crystals, *Nature communications* **7**, 13807 (2016).
- [40] L. Zhang, M. Zhang, L. Wang, C. Zhou, Z. Zhang, Y. Yao, L. Zhang, D. Xue, X. Lou, and X. Ren, Phase transitions and the piezoelectricity around morphotropic phase boundary in $\text{Ba}(\text{Zr}_{0.2}\text{Ti}_{0.8})\text{O}_3$ - $\text{Ba}(\text{Ca}_{0.7}\text{Ca}_{0.3})\text{TiO}_3$ lead-free solid solution, *Applied Physics Letters* **105**, 162908 (2014).
- [41] G. Singh, V. Sathe, and V. Tiwari, Investigation of rhombohedral-to-tetragonal phase transition in $0.5\text{Ba}(\text{Ti}_{0.8}\text{Zr}_{0.2})\text{O}_3$ - $0.5(\text{Ba}_{0.7}\text{Ca}_{0.3})\text{TiO}_3$ lead-free ferroelectric using micro-Raman scattering, *Journal of Electronic Materials* **46**, 4976 (2017).
- [42] K. Datta, K. Brajesh, R. Ranjan, and B. Mihailova, Adaptive dipolar correlation in ferroelectric $x(\text{Ba}_{0.7}\text{Ca}_{0.3})\text{TiO}_3$ -($1-x$) $\text{Ba}(\text{Zr}_{0.2}\text{Ti}_{0.8})\text{O}_3$, *Physical Review B* **102**, 060102 (2020).
- [43] V. Buscaglia, S. Tripathi, V. Petkov, M. Dapiaggi, M. Deluca, A. Gajović, and Y. Ren, Average and local atomic-scale structure in $\text{BaZr}_{1-x}\text{Ti}_x\text{O}_3$ ($x = 0.10, 0.20, 0.40$) ceramics by high-energy x-ray diffraction and Raman spectroscopy, *Journal of Physics: Condensed Matter* **26**, 065901 (2014).
- [44] B. C. Keswani, D. Saraf, S. Patil, A. Kshirsagar, A. James, Y. Kolekar, and C. Ramana, Role of a-site Ca and b-site Zr substitution in BaTiO_3 lead-free compounds: Combined experimental and first principles density functional theoretical studies, *Journal of Applied Physics* **123**, 204104 (2018).
- [45] U. Pasha, H. Zheng, O. Thakur, A. Feteira, K. Whittle, D. Sinclair, and I. Reaney, In situ Raman spectroscopy of a-site doped barium titanate, *Applied physics letters* **91**, 062908 (2007).
- [46] H. Uršič and U. Prah, Investigations of ferroelectric polycrystalline bulks and thick films using piezoresponse force microscopy, *Proceedings of the Royal Society A* **475**, 20180782 (2019).
- [47] K. Kim and J. E. Huber, In situ observation of ferroelastic domain evolution in a near-morphotropic $\text{Pb}(\text{Zr}, \text{Ti})\text{O}_3$ ceramic by piezoresponse force microscopy, *Journal of the European Ceramic Society* **35**, 1459 (2015).
- [48] M. Otonicar, H. Ursic, M. Dragomir, A. Bradesko, G. Esteves, J. Jones, A. Bencan, B. Malic, and T. Rojac, Multiscale field-induced structure of $(1-x)\text{Pb}(\text{Mg}_{1/3}\text{Nb}_{2/3})\text{O}_3$ - xPbTiO_3 ceramics from combined techniques, *Acta Materialia* **154**, 14 (2018).
- [49] J. Yao, W. Ge, L. Luo, J. Li, D. Viehland, and H. Luo, Hierarchical domains in $\text{Na}_{1/2}\text{Bi}_{1/2}\text{TiO}_3$ single crystals: Ferroelectric phase transformations within the geometrical restrictions of a ferroelastic inheritance, *Applied Physics Letters* **96**, 222905 (2010).
- [50] H. Wang, J. Zhu, N. Lu, A. Bokov, Z.-G. Ye, and X. Zhang, Hierarchical micro-/nanoscale domain structure in mc phase of $(1-x)\text{Pb}(\text{Mg}_{1/3}\text{Nb}_{2/3})\text{O}_3$ - $x\text{PbTiO}_3$ single crystal, *Applied physics letters* **89**, 042908 (2006).
- [51] K. Fang, W. Jing, and F. Fang, Multi-scale domain structure observation and piezoelectric responses for $[001]$ -oriented $\text{PbMn}_{0.33}\text{PbTi}_{0.67}$ single crystal, *Journal of the American Ceramic Society* **102**, 7710 (2019).
- [52] J. Yao, L. Yan, W. Ge, L. Luo, J. Li, D. Viehland, Q. Zhang, and H. Luo, Evolution of domain structures in $\text{Na}_{1/2}\text{Bi}_{1/2}\text{TiO}_3$ single crystals with BaTiO_3 , *Physical Review B* **83**, 054107 (2011).
- [53] C. Hu, X. Meng, M.-H. Zhang, H. Tian, J. E. Daniels, P. Tan, F. Huang, L. Li, K. Wang, J.-F. Li, *et al.*, Ultra-large electric field-induced strain in potassium sodium niobate crystals, *Science advances* **6**, eaay5979 (2020).
- [54] A. Khachatryan, Ferroelectric solid solutions with morphotropic boundary: Rotational instability of polarization, metastable coexistence of phases and nanodomain adaptive states, *Philosophical Magazine* **90**, 37 (2010).
- [55] M. Hinterstein, J. Rouquette, J. Haines, P. Papet, M. Knapp, J. Glaum, and H. Fuess, Structural description of the macroscopic piezo- and ferroelectric properties of lead zirconate titanate, *Physical review letters* **107**, 077602 (2011).
- [56] R. Guo, L. Cross, S. Park, B. Noheda, D. Cox, and G. Shirane, Origin of the high piezoelectric response in $\text{PbZr}_{1-x}\text{Ti}_x\text{O}_3$, *Physical Review Letters* **84**, 5423 (2000).
- [57] H. Liu, J. Chen, L. Fan, Y. Ren, Z. Pan, K. Lalitha, J. Rödel, and X. Xing, Critical role of monoclinic po-

- larization rotation in high-performance perovskite piezoelectric materials, *Physical review letters* **119**, 017601 (2017).
- [58] M. C. Ehmke, N. H. Khansur, J. E. Daniels, J. E. Blendell, and K. J. Bowman, Resolving structural contributions to the electric-field-induced strain in lead-free $(1-x)\text{Ba}(\text{Zr}_{0.2}\text{Ti}_{0.8})\text{O}_3-x(\text{Ba}_{0.7}\text{Ca}_{0.3})\text{TiO}_3$ piezoceramics, *Acta Materialia* **66**, 340 (2014).
- [59] D. Nuzhnyy, J. Petzelt, M. Savinov, T. Ostapchuk, V. Bovtun, M. Kempa, J. Hlinka, V. Buscaglia, M. Buscaglia, and P. Nanni, Broadband dielectric response of $\text{Ba}(\text{Zr}, \text{Ti})\text{O}_3$ ceramics: from incipient via relaxor and diffuse up to classical ferroelectric behavior, *Physical Review B* **86**, 014106 (2012).
- [60] O. Noblanc, P. Gaucher, and G. Calvarin, Structural and dielectric studies of $\text{Pb}(\text{Mg}_{1/3}\text{Nb}_{2/3})\text{O}_3\text{-PbTiO}_3$ ferroelectric solid solutions around the morphotropic boundary, *Journal of applied physics* **79**, 4291 (1996).
- [61] R. D. Shannon, Revised effective ionic radii and systematic studies of interatomic distances in halides and chalcogenides, *Acta crystallographica section A: crystal physics, diffraction, theoretical and general crystallography* **32**, 751 (1976).
- [62] D. Amoroso, A. Cano, and P. Ghosez, First-principles study of $(\text{Ba}, \text{Ca})\text{TiO}_3$ and $\text{Ba}(\text{Ti}, \text{Zr})\text{O}_3$ solid solutions, *Physical Review B* **97**, 174108 (2018).
- [63] D. Amoroso, A. Cano, and P. Ghosez, Interplay between Ca - and Ti -driven ferroelectric distortions in $(\text{Ba}, \text{Ca})\text{TiO}_3$ solid solutions from first-principles calculations, *Applied Physics Letters* **114**, 092902 (2019).
- [64] Y. Kuroiwa, S. Aoyagi, A. Sawada, J. Harada, E. Nishibori, M. Takata, and M. Sakata, Evidence for Pb-O covalency in tetragonal PbTiO_3 , *Physical review letters* **87**, 217601 (2001).
- [65] A. Tagantsev, K. Vaideswaran, S. Vakhrušev, A. Filimonov, R. Burkovsky, A. Shaganov, D. Andronikova, A. Rudskoy, A. Baron, H. Uchiyama, *et al.*, The origin of antiferroelectricity in PbZrO_3 , *Nature communications* **4**, 1 (2013).
- [66] D. Cao, I.-K. Jeong, R. Heffner, T. Darling, J.-K. Lee, F. Bridges, J.-S. Park, and K.-S. Hong, Local structure study of the off-center displacement of Ti and Zr across the morphotropic phase boundary of $\text{Pb}(\text{Zr}_{1-x}\text{Ti}_x)\text{O}_3$ ($x=0.40, 0.47, 0.49, 0.55$), *Physical Review B* **70**, 224102 (2004).
- [67] D. Phelan, C. Stock, J. A. Rodriguez-Rivera, S. Chi, J. Leão, X. Long, Y. Xie, A. A. Bokov, Z.-G. Ye, P. Ganesh, *et al.*, Role of random electric fields in relaxors, *Proceedings of the National Academy of Sciences* **111**, 1754 (2014).
- [68] D. Wang, J. Hlinka, A. Bokov, Z.-G. Ye, P. Ondrejčková, J. Petzelt, and L. Bellaiche, Fano resonance and dipolar relaxation in lead-free relaxors, *Nature communications* **5**, 5100 (2014).
- [69] A. Akbarzadeh, S. Prosandeev, E. J. Walter, A. Al-Barakaty, and L. Bellaiche, Finite-temperature properties of $\text{Ba}(\text{Zr}, \text{Ti})\text{O}_3$ relaxors from first principles, *Physical review letters* **108**, 257601 (2012).
- [70] J. Petzelt, D. Nuzhnyy, M. Savinov, V. Bovtun, M. Kempa, T. Ostapchuk, J. Hlinka, G. Canu, and V. Buscaglia, Broadband dielectric spectroscopy of $\text{Ba}(\text{Zr}, \text{Ti})\text{O}_3$: dynamics of relaxors and diffuse ferroelectrics, *Ferroelectrics* **469**, 14 (2014).
- [71] J. Petzelt, D. Nuzhnyy, V. Bovtun, M. Kempa, M. Savinov, S. Kamba, and J. Hlinka, Lattice dynamics and dielectric spectroscopy of BZT and NBT lead-free perovskite relaxors—comparison with lead-based relaxors, *Phase Transitions* **88**, 320 (2015).
- [72] F. Li, S. Zhang, Z. Xu, and L.-Q. Chen, The contributions of polar nanoregions to the dielectric and piezoelectric responses in domain-engineered relaxor- PbTiO_3 crystals, *Advanced Functional Materials* **27**, 1700310 (2017).
- [73] F. Li, S. Zhang, D. Damjanovic, L.-Q. Chen, and T. R. Shrout, Local structural heterogeneity and electromechanical responses of ferroelectrics: learning from relaxor ferroelectrics, *Advanced Functional Materials* **28**, 1801504 (2018).